Magnetic Resonance in Medicine 52:1239–1245 (2004)

Measurement and Correction of Respiration-Induced B_0 Variations in Breast ^{1}H MRS at 4 Tesla

Patrick J. Bolan,* Pierre-Gilles Henry, Eva H. Baker, Sina Meisamy, and Michael Garwood

Respiratory motion is well known to cause artifacts in magnetic resonance spectroscopy (MRS). In MRS of the breast, the dominant artifact is not due to motion of the breast itself, but rather it is produced by B_0 field distortions associated with respiratory motion of tissues in the chest and abdomen. This susceptibility artifact has been reported to occur in the brain, but it is more apparent in the breast due to the anatomic proximity of the lungs. In the breast, these B_0 distortions cause shot-to-shot frequency shifts, which vary an average of 24 Hz during a typical ^{1}H MRS scan at 4 T. This variation can be corrected retrospectively by frequency shifting individual spectra prior to averaging. If not corrected, these shifts reduce spectral resolution and increase peak fitting errors. This work demonstrates the artifact, describes a method for correcting it, and evaluates its impact on quantitative spectroscopy. When the artifact is not corrected, quantification errors increase by an average of 28%, which dramatically impacts the ability to measure metabolite resonances at low signal-to-noise ratios. Magn Reson Med 52:1239–1245, 2004. © 2004 Wiley-Liss, Inc.

Key words: respiration; susceptibility; MRS; breast cancer

INTRODUCTION

Physiologic motion associated with respiratory and cardiac cycles is known to cause artifacts in magnetic resonance spectroscopy (MRS). The situation is most severe when the tissue being studied experiences gross motion, causing the voxel(s) to be displaced from the intended position. This is common in thoracic and abdominal MRS, where techniques such as triggering (1,2), breath-holding (3), and retrospective data rejection (4) can be used to reduce the impact of gross displacement. When motions are small relative to the voxel size, this displacement artifact is negligible. However, these small-scale motions can produce phase variations between consecutively acquired free induction decays (FIDs). If these are not corrected prior to averaging the FIDs, destructive interference will cause a decrease of signal intensities. These phase variations can be corrected by retrospectively phasing individual spectra prior to averaging. The reference for the phase correction can be derived from physiologic monitoring (5), from a navigator echo (6,7), or from resonances in the data itself (8–12). Alternatively, phase variations can be avoided altogether by using physiologic triggering (13).

MRS has been increasingly used in adjunct with breast MRI for diagnosing cancer and monitoring response to cancer treatments. Malignant breast lesions have been shown to contain elevated levels of choline-containing compounds, which appear as a single resonance at 3.2 ppm in ^{1}H MRS (14). Typical breast MRS studies are performed with the subject lying prone in the magnet and with a coil designed to support the breast. Consequently, motion of the breast tissue is restricted, and gross displacements are usually less than 1–2 mm. This motion produces the small edge artifacts that are commonly seen in subtraction images of dynamic contrast enhanced breast studies. Although these displacements are small compared to the typical ^{1}H MRS voxel size (~10 mm), they can still produce substantial phase variations.

Another effect of respiratory motion can occur even when the tissue within a voxel is completely immobile. As the lungs and diaphragm move during respiration, they create time-dependent B_0 variations that extend far from the chest (15,16). This was demonstrated by Raj et al., who showed that respiratory motion can produce significant signal fluctuations in EPI images acquired in a phantom placed adjacent to a subject's head (17). These B_0 fluctuations produce frequency shifts in acquired spectra. Previous studies in brain MRS have shown that this artifact degrades the quality of spectra averaged over multiple acquisitions by reducing spectral resolution and increasing quantitative fitting errors (11,12,18). In the brain, the magnitude of these shifts is on the order of 0.01 ppm, with reports of 0.8–2 Hz at 3 T (12,18) and 1.5–4 Hz at 7 T (16). These shifts are small relative to the spectral linewidth, so the spectral degradation caused by frequency shifts is a minor effect compared to the signal loss caused by phase variations (11). However, the magnitude of respiratory-induced B_0 shifts increases with proximity to the chest (16,19). As is demonstrated in this work, the magnitude of these shifts in the breast is typically 0.1 ppm—10× greater than that measured in the brain.

This article aims to measure this artifact and evaluate its impact on quantitative breast MRS. Breath-hold imaging and physiologic monitoring were used to determine the relationship between MRS frequency shifts and respiration. Spectral fitting and quantification were performed

Center for Magnetic Resonance Research and Department of Radiology, University of Minnesota School of Medicine, Minneapolis, Minnesota

Presented in part at 2002 ISMRM Annual Meeting, Honolulu, Hawaii.

Grant sponsors: NIH; Grant numbers: RR08079, CA92004, RR00400, and CA77398; Grant sponsor: DOD Breast Cancer Research program; Grant numbers: DAMD 17–01-1–0331; Grant sponsor: Lillian Quist–Joyce Henline Chair in Biomedical Research; Grant sponsor: University of Minnesota Doctoral Dissertation Fellowship

* Correspondence to: Patrick J. Bolan, Ph.D., Center for Magnetic Resonance Research, 2021 Sixth Street SE, Minneapolis, MN 55455. E-mail: bolan@cmrr.umn.edu

Received 31 March 2004; revised 24 June 2004; accepted 30 June 2004

DOI 10.1002/mrm.20277

Published online in Wiley InterScience (www.interscience.wiley.com).

both with and without retrospective frequency correction to demonstrate that fitting errors decrease significantly when frequency correction is performed.

METHODS

All measurements were performed with a research 4-T system, consisting of a 90-cm bore magnet (model 4 T-900, Oxford Magnet Technology, Oxfordshire, UK) with a clinical gradient system (Model Sonata, Siemens, Erlangen, Germany) interfaced with an imaging spectrometer (Model Unity Inova, Varian, Palo Alto, CA). Several different single-breast quadrature transmit/receive RF surface coils of similar design were used to accommodate different breast sizes (20). The coils were mounted onto a custom-built patient table designed for unilateral, prone breast studies. In several examinations, a pneumatic belt was wrapped around the thorax just below the breasts to acquire chest expansion data. The subject population for this study included both normal volunteers and patients with either a suspicious breast lesion or a known breast cancer. The study was approved by our institutional review board, and informed consent was obtained prior to performing each experiment. All processing of images and spectra was performed using Matlab (The Mathworks, Natick, MA).

Assessment of Respiratory Effects

Breath-hold imaging was performed in three normal subjects to evaluate the spatial variation of respiration artifacts. Single-slice gradient echo images (matrix = 256 × 128, slice thickness = 5 mm, field of view = 14 cm, TR/TE = 50/15 ms) were acquired during breath holds at both maximum inspiration and maximum expiration. Maps of the phase difference ($\Delta\phi$) between inspiration and expiration were created by dividing the two complex images and extracting the phase. A mask for the high signal-to-noise region was created by thresholding the magnitude image and applying spatial smoothing (using Matlab's *bwmorph* function). The $\Delta\phi$ map was smoothed (median filter, 8 × 8 kernel) and manually unwrapped to correct phase discontinuities greater than π. The $\Delta\phi$ map was then converted into a frequency-shift map $\Delta\nu = \Delta\phi/(2\pi\mathrm{TE})$, expressed in hertz.

Spectroscopy Acquisition

In vivo spectra were recorded as part of our standard breast MR protocol, consisting of a dynamic contrast-enhanced MRI study followed by single-voxel spectroscopy. After localized shimming and power calibration, single-voxel spectra were acquired using localization by adiabatic selective refocusing (LASER) (21). Water suppression was performed using variable pulse power and optimized relaxation delays (VAPOR) (22). TE averaging (23) was used to reduce lipid sideband artifacts (TE = 45–196 ms in N = 64 or 128 increments, TR = 3 s). Each FID was individually saved—no averaging was performed until processing. A fully relaxed, single-shot spectrum with no water suppression was also acquired from each voxel to provide a reference water resonance.

Postprocessing

Spectra were postprocessed and the levels of total choline-containing compounds (tCho) were calculated using a fully automated method described previously (14) and summarized briefly here. For postprocessing, each individually saved FID was automatically corrected for DC offset and variation of zero-order phase. Frequency shifts between individual FIDs were calculated using a frequency-domain cross-correlation method (18). Each FID was shifted in frequency by multiplying the time-domain data by a linear phase function, $\exp(i\cdot 2\pi\cdot\Delta\nu\cdot t)$. The frequency shift magnitude $\Delta\nu$ was chosen to maximize the cross-correlation (evaluated in modulus mode and in the frequency domain) between the spectrum and a reference spectrum (arbitrarily, the first in the series). The variability of $\Delta\nu$ over all FIDs in a single-voxel acquisition was characterized by its range $R(\Delta\nu)$ and SD $\sigma(\Delta\nu)$.

The quantification method used the unsuppressed water resonance as an internal reference to normalize the amplitude of the tCho resonance and obtain an estimate of the concentration (denoted [tCho]) expressed in molal units (mmol/kg-water). Spectral fitting was performed one resonance at a time by fitting a Voigt line shape to a narrow band of the frequency domain (0.4 ppm) centered around the resonance. The fitting error was estimated using the Cramér–Rao minimum variance bound, which was calculated using the covariance matrix provided by the fitting routine. The SD of the fitting error, σ_{tCho}, was normalized to the amplitude of the tCho resonance and expressed as a percentage. This error was also used to establish the detectability threshold as follows: if σ_{tCho} was greater than 100% then the tCho resonance was considered undetectable.

Quantitative Spectroscopy

A retrospective analysis was performed to evaluate whether the frequency correction impacts the results of spectral quantification. In vivo breast MRS data acquired from subjects over a 2-year period were included in this study. The subjects included 24 patients with biopsy-confirmed cancer undergoing neoadjuvant chemotherapy, 112 patients with a suspicious breast lesion evaluated immediately pre- or postbiopsy, and 6 normal volunteers. A total of 714 TE-averaged spectra were acquired from all 142 subjects in 253 studies. A subset of 280 spectra were chosen for this retrospective analysis by removing 9 spectra with visible artifacts, 151 spectra with lipid content greater than the previously specified threshold (14), and 275 spectra with no detectable tCho resonance. These 280 spectra were processed and quantified both with and without frequency correction. Omission of the frequency correction step is equivalent to the common practice of automatically averaging FIDs prior to postprocessing.

RESULTS

Assessment of Respiratory Effects

Figure 1 is a representative data set showing sagittal images from one breath-hold study of a normal breast. Magnitude images acquired during maximum inspiration (Fig.

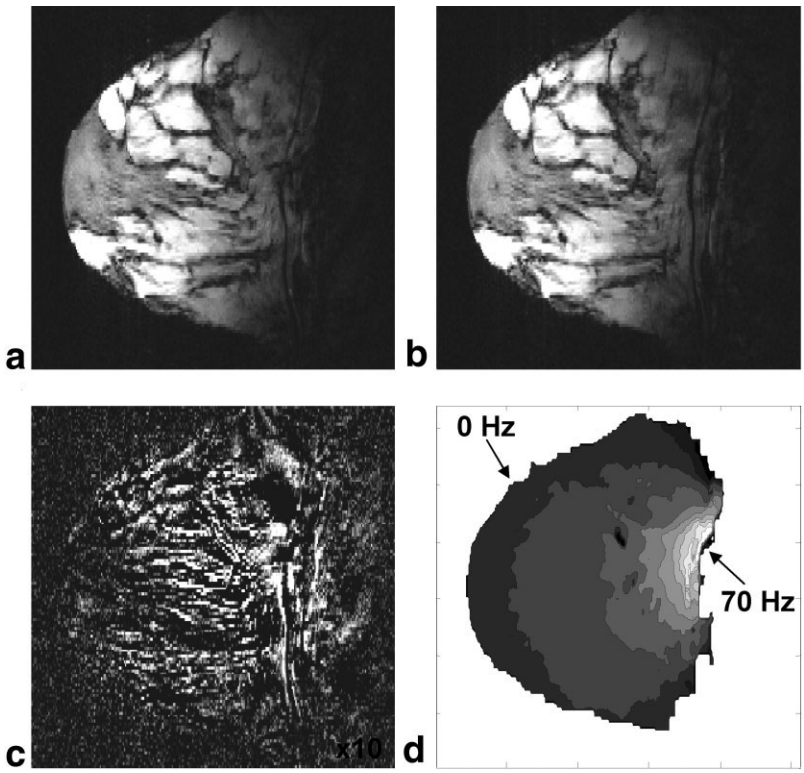

FIG. 1. Demonstration of respiration artifacts by MR imaging. The top row shows sagittal gradient-echo images of a subject's left breast during breath-holds at (**a**) maximum inspiration and (**b**) maximum expiration. The magnitude difference between these two images is shown in **c**, scaled by a factor of 10, showing that there was little gross motion of the breast during respiration. The phase difference between **a** and **b** was converted into a $\Delta\nu$ map, shown in **d**, with contour lines every 10 Hz. The frequency shift varied from <10 Hz at the skin to 70 Hz nearest the chest wall.

1a) and maximum expiration (Fig. 1b) are very similar. The magnitude difference image (Fig. 1c) shows that the gross motion of the breast was small during respiration, causing only small edge artifacts. The phase difference between inspiration and expiration was converted into a map of frequency shift, $\Delta\nu$, shown in Fig. 1d. The $\Delta\nu$ map shows a strong spatial dependence, with the greatest effect (~70 Hz) closest to the chest wall. A voxel placed in the center of the breast would have experienced a shift of 10–20 Hz between maximum inspiration and expiration. Similar $\Delta\nu$ maps were reproduced in each breath-hold subject. The largest frequency shifts were nearest the chest wall in both left and right breasts and in axial and sagittal orientations.

The relationship between MRS frequency shifts and the respiratory cycle is shown in Fig. 2. In the figure, the dots indicate frequency shifts measured from NMR spectra using the cross-correlation method described above. The line shows the chest expansion measured by the pneumatic belt, scaled and shifted to match the frequency shifts. The good agreement between these data sets indicates that the frequency shifts were most likely caused by respiration rather than by cardiac motion. This also suggests that physiologic monitoring of the chest expansion could be used to correct frequency shifts in the spectra.

Frequency Correction Examples

The frequency correction method is demonstrated in Fig. 3, which shows a series of single-shot (NEX = 1), fixed TE (TE = 45 ms) spectra acquired from a malignant lesion. The frequency variation evident in the uncorrected spectra (Fig. 3a) is removed after frequency correction (Fig. 3b). After averaging and fitting both the corrected and uncorrected series, the corrected spectrum (Fig. 4a, top) had improved spectral resolution, increased tCho amplitude, and decreased fitting error as compared to the uncorrected spectrum (Fig. 4a, bottom). This example is not representative of a typical acquisition, because the SNR was atypically high and TE averaging was not used. However, this case provides a clear example of the impact of the frequency correction method.

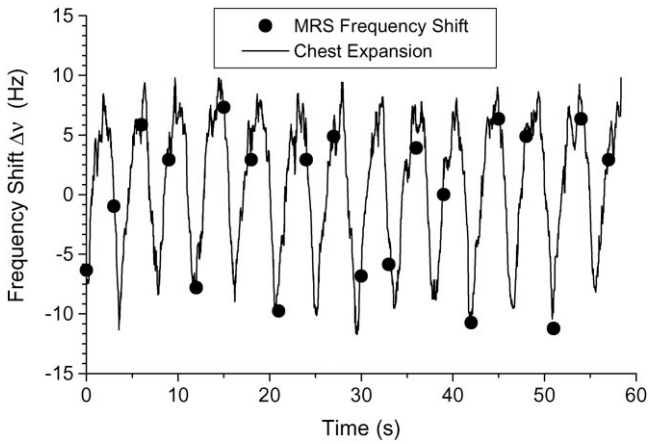

FIG. 2. Demonstration of the relationship between spectral frequency shifts and chest expansion. The subject was asked to breathe normally while a series of localized, unsuppressed spectra were acquired with TR = 3 s. The line shows the (smoothed) chest expansion as measured with a pneumatic chest bellows. The dots show the magnitude of frequency shifts measured using the cross-correlation method on the spectra at corresponding time points. The magnitude of the chest expansion data were manually scaled to match the measured frequency offsets.

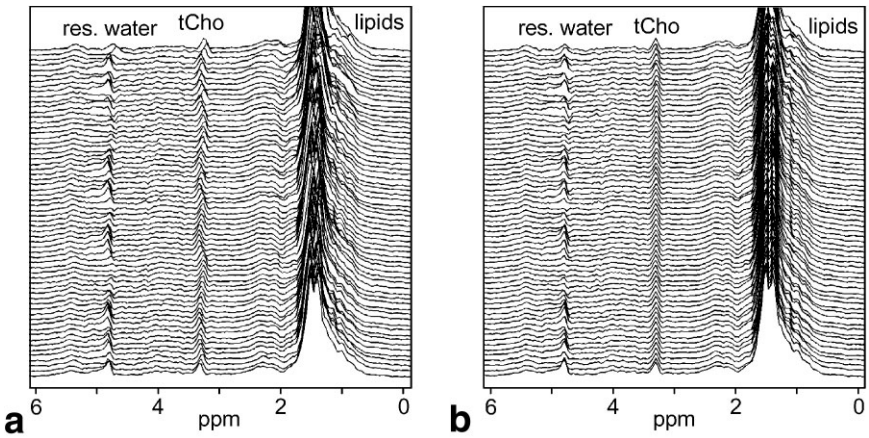

FIG. 3. Demonstration of frequency correction. A series of 64 identical single-shot (NEX = 1), water-suppressed, in vivo spectra (TR/TE = 3000/45 msec) acquired during normal respiration are shown (**a**) prior to and (**b**) after frequency correction using the cross-correlation method. The measured frequency shifts in this acquisition varied over a range of $R(\Delta\nu)$ = 23.0 Hz with a SD of $\sigma(\Delta\nu)$ 4.9 Hz. Note that these data are not TE-averaged and have an unusually high signal-to-noise ratio.

Several representative examples of TE-averaged acquisitions are shown in Figs. 4b–d, with and without frequency correction. Figures 4b and 4c show how the magnitude of the frequency variation can affect the spectral quality. Both are good-quality spectra with resonance from several metabolites in addition to tCho. In Fig. 4b, the corrected and uncorrected spectra appear similar because the frequency variation was relatively small. In Fig. 4c, where the frequency variation was larger, the corrected data clearly show improved spectral resolution. Fig. 4d shows a case where tCho was detectable with frequency correction and not detectable (using the $\sigma_{tCho} < 100\%$ criterion) when the frequency correction was omitted.

Quantitative Spectroscopy

The quantification procedure was performed using frequency correction on the full set of 280 TE-averaged spectra with a detectable tCho resonance. These spectra were then reprocessed with the frequency correction step removed. The resultant spectral broadening generally increased the Cramér–Rao errors, making the tCho resonance undetectable in 69/280 (25%) spectra based on the $\sigma_{tCho} < 100\%$ criterion. Of the remaining 211 spectra, the calculated [tCho] values, shown in Fig. 5a, did not change (P = 0.28, two-tailed t test). The errors, shown in Fig. 5b, were an average of 28% larger when the frequency correction

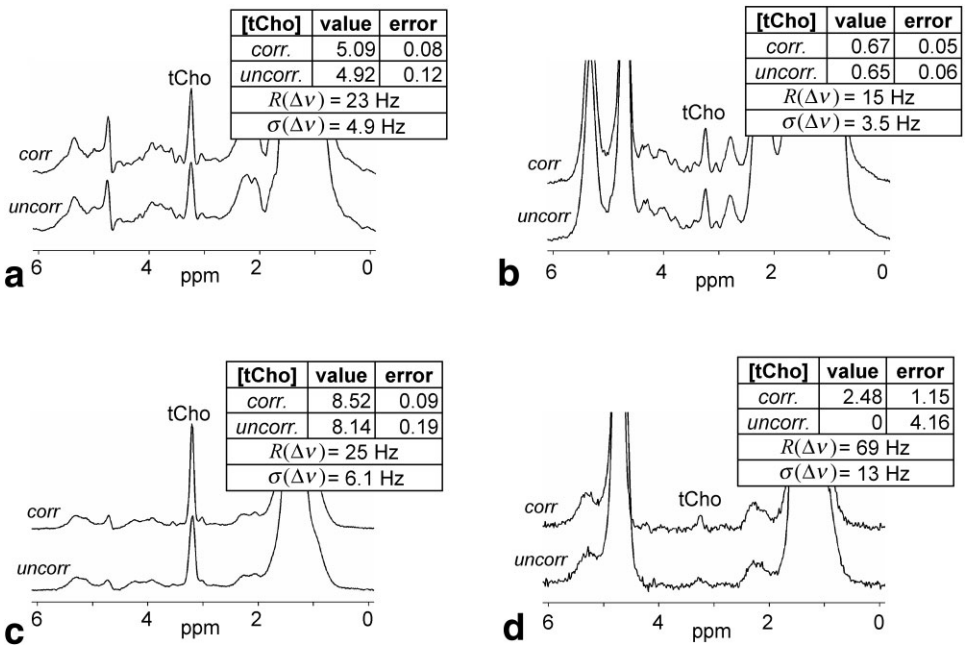

FIG. 4. Impact of frequency correction on spectral quantification. Each pair of spectra shown in **a**–**d** are averaged from the same acquired data but processed with (top) and without (bottom) frequency correction. The inset tables show calculated [tCho] concentrations and fitting errors (mmol/kg) based on the method in Ref 14 for both corrected an uncorrected spectra. The range $R(\Delta\nu)$ and SD $\sigma(\Delta\nu)$ of the frequency variation over each acquisition is also shown. The pair in **a** are averaged from the single-TE arrays shown in Figs. 3(**a**) and (**b**). Pairs **b**–**d** are examples of TE-averaged spectra (TE = 45–196 ms in 128 increments, TR = 3 s), demonstrating cases where the effect of frequency correction is relatively small (**b**), moderate (**c**), and large (**d**). In the uncorrected spectrum of **d**, the normalized fitting error (σ_{tCho} = 140%) exceeded the detection threshold, so in this case a tCho resonance is only detectable with frequency correction.

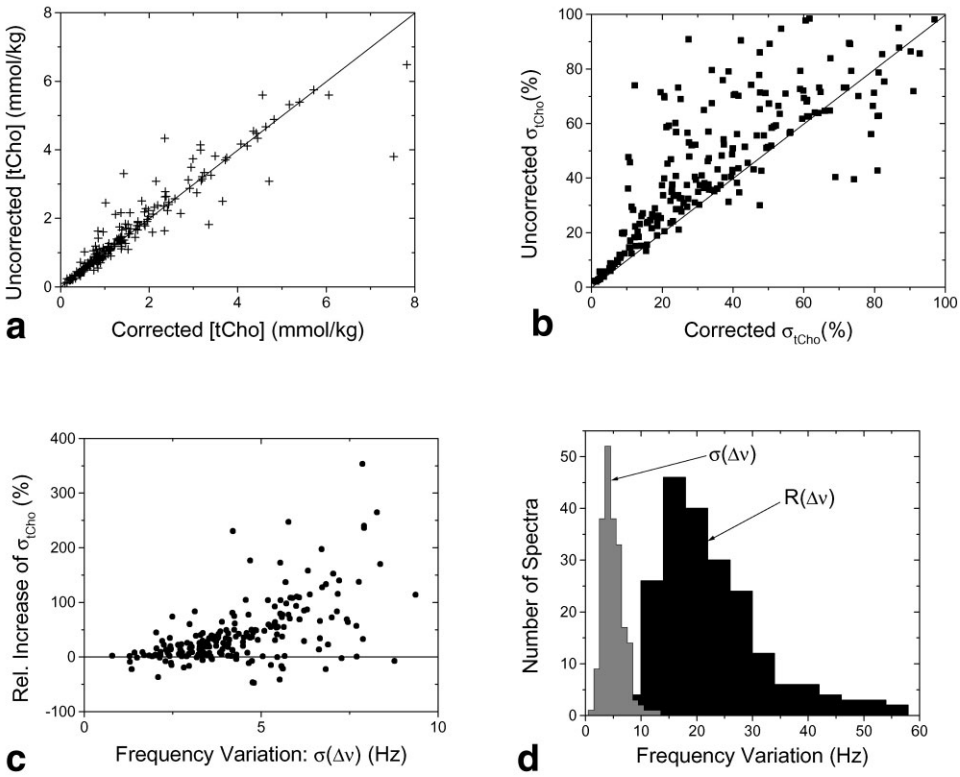

FIG. 5. Quantitative impact of frequency correction on quantification error evaluated in a series of 280 in vivo spectra. (**a**) Plot compares the total tCho concentration ([tCho]) when processed with and without frequency correction. There is no significant difference ($P = 0.28$). (**b**) Plot shows the fitting errors (normalized SD based on Cramér–Rao lower bounds) when processed with and without frequency correction. On average, the error is 28% larger without frequency correction. (**c**) The increase in error is plotted against the SD of $\Delta\nu$ for each spectrum. (**d**) Histograms for the range $R(\Delta\nu)$ and SD $\sigma(\Delta\nu)$ of the frequency variation in all 280 spectra.

was omitted. As expected, the increase in error was greater when the magnitude of the frequency variation was larger, as shown in Fig. 5c. The range and SD of the frequency variation are shown as histograms in Fig. 5d. The mean range of the frequency variation $R(\Delta\nu)$ was 24 Hz (0.14 ppm).

DISCUSSION

This study demonstrates that the correction of respiratory-induced frequency variations improves the quality of breast ^{1}H MRS at 4 T. The proposed method of retrospectively correcting frequency shifts prior to averaging is applicable in cases where gross displacement of the tissue is relatively small, but B_0 variations are substantial. This scenario is typical of high-field breast MRS, in which breast motion is restricted by the coil platform, but frequency variations are large due to the proximity of the lungs. These frequency variations will be greater at higher magnetic fields because susceptibility-induced field distortions scale with field strength. The impact of this artifact has not been reported at 1.5 T, presumably because the susceptibility effects are less apparent than at 4 T.

The magnitude of the respiration-induced frequency variation measured in the breast at 4 T typically ranges from 10 to 30 Hz, with a mean of 24 Hz found in this study. The magnitude depends on the position of the voxel within the breast. All the $\Delta\nu$ maps acquired in this study showed a general trend of increased frequency variation closer to the chest wall. Further studies are required to measure the full spatial dependence of $\Delta\nu$ and determine if cardiac motion contributes to the effect. Other factors not explicitly measured but expected to affect the artifact include depth of respiration, chest size, and body composition. If left uncorrected, frequency variations during an acquisition will cause a blurring of the averaged spectrum, reducing the effective spectral resolution and distorting the line shape.

Although the qualitative impact of frequency shifts on breast spectra is often not dramatic, particularly when the frequency shifts are small, the quantitative impact of this artifact is always present. Even small frequency variations produce an increase in fitting errors (Fig. 5c), effectively decreasing the sensitivity of spectroscopic measurements. This is most critical when fitting metabolites at low signal-to-noise ratios, which is common in breast MRS.

The increased error is likely explained by the increased line widths produced by uncorrected frequency variation. In general, peak amplitude estimation errors are larger for broader resonances. This has been shown analytically for the case of a simple Lorentzian resonance (24). The Voigt line-shape model used in this work is equivalent to a Lorentzian line shape convolved with a Gaussian frequency blurring, which enables the model to account for frequency variations without introducing bias in the amplitude estimates. These properties were verified by simulating spectral data sets with random frequency variations: as the magnitude of frequency variation increased, the amplitude estimates did not change, but the amplitude *error* estimates did increase (data not shown). These results are consistent with the in vivo data shown in Fig. 5a–c. Although not evaluated in this work, it is expected that other spectral fitting methods would produce similar results, provided a sufficiently flexible line-shape model is used. This is supported by a previous study (11) that showed an increase in fitting errors but no effect on peak amplitudes when fitting spectra with the LCModel soft-

ware package (25), which also uses a flexible line-shape model.

There are a number of approaches for handling respiration-induced frequency variations. In principle, the artifact can be avoided altogether using respiratory triggering or breath-hold acquisitions. These methods are error-prone and are less efficient in use of machine time, but are necessary for spectroscopic editing techniques requiring precise frequency selectivity. Alternatively, the frequency distortion function $\Delta\nu(t)$ can be estimated and retrospectively corrected prior to averaging spectra, as is commonly done for phase variations. The $\Delta\nu(t)$ function can be estimated from either physiologic monitoring, MR navigator signals, or directly from the acquired data. Physiologic monitoring, typically done with chest expansion bellows or ECGs, is least direct and requires careful processing to properly denoise and detrend the data. Using navigator signals has the disadvantage that there is typically a delay between the navigator acquisition and the actual FID; the length of the delay may be significant when compared to the respiratory period. Although not shown, we also developed and tested a version of LASER with an interleaved small-flip-angle STEAM acquisition immediately following the metabolite acquisition period, similar to the method described by Thiel et al. (7). This also worked acceptably, but it was not as effective as the cross-correlation method, probably due to the delay between the navigator echo and the measured FID (350 ms). A nonlocalized navigator with a shorter delay was also tested, but these shift measurements did not correlate well with the localized shifts.

Extracting $\Delta\nu(t)$ directly from the data, as in this work, is the most direct way of measuring the artifact. This approach requires sufficient SNR in each acquisition to measure frequency shifts. Numerous methods have been proposed for measuring $\Delta\nu$ between consecutive spectra, including cross-correlation, frequency-referencing a single resonance, time domain fitting, and principal component analysis (18,26). The time domain method does not work well with TE-averaged data because the initial portion of each individual FID is distorted by B_0 modulations, which are corrected only after averaging. The single resonance referencing method (with the 1.3-ppm lipid) and cross-correlation method worked comparably, but the cross-correlation method was overall more robust because it uses the full spectral information. Using the residual water resonance as a frequency reference has been proposed by other groups (10,12). This approach is also feasible provided the water suppression is adjusted properly and has sufficient bandwidth to avoid frequency-dependent line-shape variations like those shown in Fig. 3a. Methods using principle component analysis may also be effective, but their applicability for TE-averaged spectra has not yet been investigated.

This study did not measure spectroscopic phase variations due to physiologic motion. Although in studies of compliant subjects there were generally no large-scale motions of the breast, small displacements of the breast (particularly near the chest wall) were visible by imaging. These small-scale breast motions may produce phase variations (10). With the TE-averaged acquisition method used in this work, the zero-order phase varies with each TE due to B_0 modulations, so phase correction is required even in the absence of motion. Therefore, separating physiologic and system sources of phase variation was not feasible.

CONCLUSION

This study reports measurements of respiratory-induced frequency variations in the breast at 4T and their impact on quantitative MRS. The average frequency variation measured over a typical acquisition was 24 Hz, which is approximately 10× greater than comparable measurements of this effect in the brain. If left uncorrected, this artifact reduces the ability to measure metabolite concentrations. In our sample of 280 spectra with a detectable tCho resonance, quantitative fitting errors increased by an average of 28%, and in 69 (25%) spectra the tCho resonance became undetectable. These results indicate that using frequency correction can improve the quality of quantitative breast ^{1}H MRS at high field.

REFERENCES

1. Dixon RM, Frahm J. Localized proton MR spectroscopy of the human kidney in vivo by means of short echo time STEAM sequences. Magn Reson Med 1994;31:482–487.
2. Felblinger J, Jung B, Slotboom J, Boesch C, Kreis R. Methods and reproducibility of cardiac/respiratory double-triggered 1H-MR spectroscopy of the human heart. Magn Reson Med 1999;42:903–910.
3. Katz-Brull R, Rofsky NM, Lenkinski RE. Breathhold Abdominal and Thoracic Proton MR Spectroscopy at 3T. Magn Reson Med 2003;50:461–467.
4. Tyszka JM, Silverman JM. Navigated single-voxel proton spectroscopy of the human liver. Magn Reson Med 1998;39:1–5.
5. Felblinger J, Kreis R, Boesch C. Effects of physiologic motion of the human brain upon quantitative 1H-MRS: analysis and correction by retro-gating. NMR Biomed 1998;11:107–114.
6. Posse S, Cuenod CA, LeBihan D. Motion artifact compensation in 1H spectroscopic imaging by signal tracking. J Magn Reson B 1993;102:222–227.
7. Thiel T, Czisch M, Elbel GK, Hennig J. Phase coherent averaging in magnetic resonance spectroscopy using interleaved navigator scans: compensation of motion artifacts and magnetic field instabilities. Magn Reson Med 2002;47:1077–1082.
8. Zhu G, Gheorghiu D, Allen PS. Motional degradation of metabolite signal strengths when using STEAM: a correction method. NMR Biomed 1992;5:209–211.
9. Ziegler A, Decorps M. Signal-to-noise improvement in in vivo spin-echo spectroscopy in the presence of motion. J Magn Reson B 1993;102:26–34.
10. Star-Lack JM, Adalsteinsson E, Gold GE, Ikeda DM, Spielman DM. Motion correction and lipid suppression for 1-H magnetic resonance spectroscopy. Magn Reson Med 2000;43:325–330.
11. Helms G, Piringer A. Restoration of motion-related signal loss and line-shape deterioration of proton MR spectra using the residual water as intrinsic reference. Magn Reson Med 2001;46:395–400.
12. Katz-Brull R, Lenkinski RE. Frame-by-frame PRESS 1H-MRS of the brain at 3 T: the effects of physiological motion. Magn Reson Med 2004;51:184–187.
13. Pattany PM, Khamis IH, Bowen BC, Goodkin K, Weaver RG, Murdoch JB, Donovon Post MJ, Quencer RM. Effects of physiologic human brain motion on proton spectroscopy: quantitative analysis and correction with cardiac gating. Am J Neuroradiol 2002;23:225–230.
14. Bolan PJ, Meisamy S, Baker EH, Lin J, Emory T, Nelson M, Everson LI, Yee D, Garwood M. In vivo quantification of choline compounds in the breast with 1H MR spectroscopy. Magn Reson Med 2003;50:1134–1143.
15. Noll DC, Schneider W. Respiration artifacts in functional brain imaging: sources of signal variation and compensation strategies. In: Proceedings of the 2nd Annual Meeting of SMR, San Francisco, 1994. p 647.

16. Van de Moortele PF, Pfeuffer J, Glover GH, Ugurbil K, Hu X. Respiration-induced B0 fluctuations and their spatial distribution in the human brain at 7 Tesla. Magn Reson Med 2002;47:888–895.
17. Raj D, Anderson AW, Gore JC. Respiratory effects in human functional magnetic resonance imaging due to bulk susceptibility changes. Phys Med Biol 2001;46:3331–3340.
18. Henry P-G, van de Moortele P-F, Giacomini E, Nauerth A, Bloch G. Field-frequency locked in vivo proton MRS on a whole-body spectrometer. Magn Reson Med 1999;42:636–642.
19. Raj D, Paley DP, Anderson AW, Kennan RP, Gore JC. A model for susceptibility artefacts from respiration in functional echo-planar magnetic resonance imaging. Phys Med Biol 2000;45:3809–3820.
20. Merkle H, DelaBarre L, Bolan PJ, Baker EH, Everson LI, Yee D, Garwood M. Transceive quadrature breast coils and applications at 4 Tesla. In: Proceedings of the 9th Annual Meeting of ISMRM, Glasgow, 2001. p 1114.
21. Garwood M, DelaBarre L. The return of the frequency sweep: designing adiabatic pulses for contemporary NMR. J Magn Reson 2001;153:155–177.
22. Tkac I, Starcuk Z, Choi IY, Gruetter R. In vivo 1H NMR spectroscopy of rat brain at 1 msec echo time. Magn Reson Med 1999;41:649–656.
23. Bolan PJ, DelaBarre L, Baker EH, Merkle H, Everson LI, Yee D, Garwood M. Eliminating spurious sidebands in 1-H MRS of breast lesions. Magn Reson Med 2002;48:215–222.
24. Yao Y-X, Pandit SM. Cramer–Rao lower bounds for a damped sinusoidal process. IEEE Trans Signal Proc 1995;43:878–885.
25. Provencher SW. Estimation of metabolite concentrations from localized in vivo proton NMR spectra. Magn Reson Med 1993;30:672–679.
26. Brown TR, Stoyanova R. NMR Spectral quantitation by principal-component analysis. II. Determination of frequency and phase shifts. J Magn Reson B 1996;112:32–43.